Journal of Alloys and Compounds 699 (2017) 938–946

Contents lists available at ScienceDirect

Journal of Alloys and Compounds

journal homepage: http://www.elsevier.com/locate/jalcom

Precipitation of TiN during solidification of AISI 439 stainless steel

Junwei Fu*, Wenxiu Qiu, Qiangqiang Nie, Yucheng Wu**

School of Materials Science and Engineering, Hefei University of Technology, Hefei, 230009, PR China

ARTICLE INFO

Article history:
Received 2 November 2016
Received in revised form
30 December 2016
Accepted 2 January 2017
Available online 3 January 2017

Keywords:
Solidification
TiN
Stainless steel
Non-equilibrium

ABSTRACT

Precipitation behavior of TiN in AISI 439 ferritic stainless steel was investigated using both thermodynamics and experiments. Calculated results using equilibrium approaches show that TiN can precipitate only when the solid-phase fraction reaches 0.2. However, TiN was observed at the surface of the water-cooled samples in our experiments, which indicates that TiN can precipitate at the initial stage of solidification when the cooling rate is sufficiently high. Therefore, in order to predict efficiently the precipitation behavior of TiN during rapid solidification, non-equilibrium effect has to be taken into account during the calculations. In this work, a model, which relates the interface temperature with the composition and growth rate at the solid/liquid interface under non-equilibrium conditions, has been developed. It is shown that the calculated results using this model are in agreement with the experimental results.

1. Introduction

Stainless steels which originate from Fe–Cr alloys are now considered as one of the most important classes of steels, and attract increasing attention in both defense and commercial products. Generally, ferritic stainless steels, austenitic stainless steels, martensitic stainless steels and duplex stainless steels are the commonly used classes of stainless steels [1]. Among these, ferritic stainless steels are more attractive because of their higher thermal conductivity, lower linear expansion, better resistance to chloride stress-corrosion cracking, pitting and crevice corrosion, and adequate high temperature resistance to oxidation. In addition, the price of ferritic stainless steels is relatively lower since no rare Ni element is added. However, ferritic stainless steels are susceptible to the intergranular corrosion (IGC) due to the formation of either chromium carbides or nitrides at the grain boundaries [2–7]. The common approach to prevent IGC in ferritic stainless steels is to reduce the content of carbon and nitrogen and add the stabilizing elements such as, Ti and/or Nb [8,9].

AISI 439 stainless steel, with stabilizing Ti element, is one of the most important classes within the Fe–17Cr ferritic stainless steels [10]. It is known that the affinity of N with Ti is much stronger than that of Fe and other metal elements [8]. If the concentrations of Ti and N in the melts of AISI 439 stainless steel are sufficiently high, TiN may form directly from the melts. Furthermore, for AISI 439 stainless steel, solutes Ti and N will be piled up at the solid/liquid interface during solidification since the equilibrium distribution coefficients of both Ti and N are less than unity. Therefore, it is much easier for TiN to form during solidification than from the melts owing to higher concentration and lower interface temperature. TiN is a brittle phase with rock salt type structure (space group $Fm\bar{3}\,m$) and its lattice parameter is $a_{TiN} = 4.27$ Å [11]. If coarse TiN precipitates at the grain boundary during solidification, it will impair the mechanical properties of the steels greatly because it is difficult for TiN to deform. Otherwise, if TiN precipitates dispersedly within the grain, it will act as the heterogeneous site and can refine the solidified microstructure of the stainless steels, aluminum alloys and titanium alloys [12–15]. So, predicting and controlling the precipitation behavior of TiN are of great importance to obtain desirable solidified microstructure and mechanical properties for ferritic stainless steels.

Great efforts have been made to understand the precipitation behavior of TiN and improve the mechanical properties of ferritic stainless steels. For the prediction of precipitation of TiN in steels, thermodynamic calculation is commonly used. According to thermodynamics, TiN precipitation is mainly determined by the product of titanium content and nitrogen content in the melts at a certain temperature.

Through extensive thermodynamic studies [16–21], it was found that under a certain temperature the product of titanium

* Corresponding author.
** Corresponding author.
E-mail addresses: hitfujw@163.com (J. Fu), ycwu@hfut.edu.cn (Y. Wu).

http://dx.doi.org/10.1016/j.jallcom.2017.01.018
0925-8388/

content and nitrogen content in the melts is a constant for a given class of steel, and the contents of N and Ti affect TiN precipitation behavior greatly. TiN would not precipitate from the melts when the product of the contents of titanium and nitrogen in the melts is less than the equilibrium concentration product under a given temperature. To predict the precipitation behavior of TiN during solidification, Brody and Fleming's model [22] is usually used to calculate the segregation behavior of solutes because the solute concentrations are increased during solidification if the equilibrium distribution coefficients are less than unity.

However, both the calculation of the product of solute concentrations in the melts and the analyses of the segregation behavior during solidification are based on the equilibrium assumption. To determine the formation of TiN in the melts, the equilibrium constant is obtained under the assumption that the Gibbs free energy change is zero. When analyzing the relationship between the interface temperature and interface composition during solidification, the Gibbs free energy change is also assumed to be zero. Equilibrium conditions are difficult to occur, and the deviation from equilibrium takes place in the common casting process. So, it is imperative for metallurgists and materials scientists to predict TiN precipitation in ferritic stainless steels. Based on the published literature, no work has been carried out to predict TiN precipitation under non-equilibrium conditions until now.

The aim of the present work is to study the precipitation of TiN in AISI 439 ferritic stainless steel during non-equilibrium cooling.

2. Experimental procedure

In this work, a commercial AISI 439 ferritic stainless steel the chemical composition of which given in Table 1 was used. The commercial stainless steel was re-melted at a temperature of 1873 K in a vacuum induction furnace, and then cast into the magnesia molds with the dimension of 40 mm inner diameter, and 150 mm height, after stabilization at 1873K for about 20 min.

In order to examine the effect of cooling rate on the precipitation behavior of TiN in AISI 439 stainless steel, after pouring the melts was cooled through three different ways, namely, furnace cooling, air cooling, and water cooling. The cooling rates of the water-cooled and furnace-cooled samples are the highest and lowest ones, respectively. Cooling rate in air lies between the cooling rates obtained in water and in furnace. The samples were electrolytically etched with 10% oxalic acid reagent after being mechanically ground and polished. The morphology and size of TiN in the microstructure were analyzed by Optical Microscopy (OM). The composition analyses were carried out by Scanning Electron Microscopy (SEM).

3. Results and discussion

3.1. Thermodynamics of TiN precipitation in Fe–Cr melts

The reaction equilibrium equation for the formation of solid TiN in liquid Fe–Cr melts can be expressed as: [17,18]

$$[\mathrm{Ti}] + [\mathrm{N}] = \mathrm{TiN}_{(s)} \tag{1}$$

The equilibrium constant for reaction (1) can be written as:

$$K_{\mathrm{TiN}} = \frac{\alpha_{\mathrm{TiN}}}{h_{\mathrm{Ti}}.h_{\mathrm{N}}} = \frac{1}{f_{\mathrm{Ti}}[\%\mathrm{Ti}]f_{\mathrm{N}}[\%\mathrm{N}]} \tag{2}$$

where h_{Ti} and h_{N} are the Henrian activities of titanium and nitrogen relative to 1 mass% standard state in liquid iron, respectively, and f_{Ti} and f_{N} are the activity coefficients of titanium and nitrogen, respectively. Under the present experimental conditions, the activity of TiN, α_{TiN}, can be considered as unity. According to Pak et al. [19], the standard Gibbs free energy change for reaction (1) can be written as:

$$\Delta G_1^{\mathrm{o}} = (-379000 + 149T)\ \mathrm{J/mol} \tag{3}$$

When the reaction reaches an equilibrium state, the relationship between equilibrium constant and standard free energy change can be expressed as:

$$\lg K_{\mathrm{TiN}} = -\frac{\Delta G_1^{\mathrm{O}}}{2.3RT} = \frac{379000 - 149T}{2.3RT} = \frac{19798}{T} - 7.78 \tag{4}$$

Based on Equations (2) and (4), the following equation can be established

$$-\frac{19798}{T} + 7.78 = \lg f_{\mathrm{Ti}} + \lg[\%\mathrm{Ti}] + \lg f_{\mathrm{N}} + \lg[\%\mathrm{N}] \tag{5}$$

According to equation (5), in order to determine the relationship between the titanium content and nitrogen content in the Fe–Cr melts at a certain temperature, the activity coefficients of titanium and nitrogen f_{Ti} and f_{N} must be known first. Generally, the activity coefficients can be obtained using Wagner theory [23]:

$$\lg f_{\mathrm{i}} = \sum_j \left(e_i^j[\%\mathrm{j}]\right) \tag{6}$$

where e_i^j is the first order interaction parameter of component j on component i. The interaction parameters, listed in Table 2, are used in the present work [18,19]. By substituting the thermodynamics parameters into Equation (6), the relationship between titanium content and nitrogen content in the Fe–Cr melts under a certain temperature can be determined using Equation (5). Fig. 1 shows the result of titanium content and nitrogen content in Fe–Cr melts under equilibrium conditions at 1873K, liquidus temperature $T_{\mathrm{L}} = 1783$ K, and solidus temperature $T_{\mathrm{S}} = 1772$ K, respectively. The content of titanium and nitrogen in the present stainless steel is denoted as point A in Fig. 1. According to thermodynamics, TiN will precipitate from the melts if the product of titanium content and

Table 2
Interaction parameters used in this work [18,19].

Parameters	1873 K	Temperature dependency
e_{Ti}^{Ti}	0.048	–
e_{Ti}^{N}	−2.041	19500/T+8.37
e_{Ti}^{Si}	−0.0256	177.5/T-0.12
e_{Ti}^{Cr}	0.028	1196/T-0.61
e_{N}^{Ti}	−0.593	−5700/T+2.45
e_{N}^{N}	0	–
e_{N}^{Si}	0.0491	−286.2/T+0.202
e_{N}^{Cr}	−0.045	−850/T+0.409

Table 1
Chemical composition of the experimental as-cast steel (wt.%).

C	Cr	Si	Ti	Mn	Ni	Al	Mo	N	Ca	O	S	P
0.01	17.65	0.28	0.24	0.27	0.18	0.02	0.03	0.0085	0.0017	0.0085	0.001	0.023

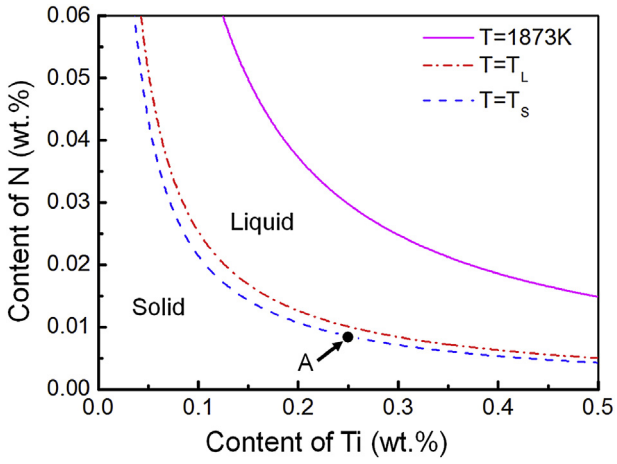

Fig. 1. Equilibrium relations between Ti content and N content in liquid iron at different temperatures.

nitrogen content in the melts is higher than the equilibrium concentration product. From Fig. 1, it is clear that the product of titanium content and nitrogen content in the present work is lower than the equilibrium concentration product at the liquidus temperature. Thus, it can be inferred that TiN would not precipitate from the melts.

3.2. Precipitation behavior of TiN during solidification under equilibrium conditions

According to the above analyses, it is clear that TiN cannot form directly from the melts. The observed TiN in the microstructure should be resulted from the solidification process. In order to understand the formation mechanism of TiN during solidification, equilibrium conditions are taken into account first. It is known that solutes will be rejected into the liquid if the equilibrium distribution coefficients of the solutes are less than unity. The solute concentration at the solid/liquid interface will increase gradually during solidification. Resultantly, melting temperature will decrease gradually with the development of solidification. The concentration of titanium and nitrogen in the melts is reduced subsequently for the class of AISI 439 stainless steel. When the concentrations of titanium and nitrogen in the melts exceed the equilibrium concentration under a temperature lower than the liquidus temperature, TiN may precipitate at this temperature. For linear solidus and liquidus lines, the solute concentration at the solid/liquid interface during solidification can be calculated from the classical lever rule as: [24]

$$C_L^* = \frac{C_0}{1-(1-k_0)f_S} \tag{7}$$

where C_L^* is solute concentration in the liquid at the solid/liquid interface, k_0 the equilibrium distribution coefficient, C_0 the initial alloy composition, and f_S the solid-phase fraction during solidification. Based on Equation (7), it is apparent that solute concentration is increased gradually with increasing the solid-phase fraction during solidification. Using the similar method, for linear liquidus and solidus and equilibrium solidification, interface temperature can be obtained as: [25]

$$T = T_0 - \frac{T_0 - T_L}{1 - f_S\frac{T_L - T_S}{T_0 - T_S}} \tag{8}$$

where T_0 is the melting point of pure solvent, T_L and T_S the liquidus and solidus of the steel studied, respectively. Using Equation (7) and the parameters listed in Table 3 [26–28], the change of the solute concentration at the solid/liquid interface during solidification can be calculated. Here, the liquidus, solidus, and liquidus slopes in Table 3 are calculated using Thermo-Calc thermodynamic software. Fig. 2 shows the relationship between the concentrations of titanium and nitrogen at the solid/liquid interface and the solid-phase fraction under equilibrium solidification. Based on Fig. 2, it can be found that titanium and nitrogen at the solid/liquid interface become enriched gradually with the increase of the solid-phase fraction. The concentration of nitrogen at the interface increases faster than that of titanium owing to its lower equilibrium distribution coefficient. This indicates that TiN may form at a certain solid-phase fraction during solidification when the concentrations of titanium and nitrogen reach the critical magnitudes required at this temperature. Usually, the precipitation behavior of TiN during solidification can be analyzed by comparing the concentration product of solutes Ti and N in the melts under a certain temperature and the concentration product during equilibrium solidification.

Using Equations (5), (6) and (8), the product of concentration of Ti and N, K'_{TiN}, in the melts can be obtained. The concentration product of Ti and N, Q_{TiN}, during equilibrium solidification can be calculated using Equation (7). Fig. 3 shows the relationship between $\lg(K'_{TiN})$ and $\lg(Q_{TiN})$ under various solid-phase fractions. It can be seen that when the solid-phase fraction reaches about 0.2, the concentration product of titanium and nitrogen during solidification is equal to the concentration product in the melts. This means that TiN should precipitate from the steel melts when the solid-phase fraction exceeds 0.2.

However, the experimental results do not support the calculation results using equilibrium approaches. In the experiments, the method to measure the distance from the surface toward the center in various samples can be schematically shown in Fig. 4. The ingots were cut longitudinally first. The samples were obtained in the radial direction, from the surface to the center, as shown in Fig. 4(a). The length of the samples is about 10 mm. During the measurement, we observed the TiN precipitations with an optical microscope from the surface to the canter in the samples, as shown in Fig. 4(b). TiN was observed at the surface of the samples cooled in water; about 1.0 mm away from the surface of the samples cooled in air and about 3.0 mm away from the surface of the samples cooled in furnace, as shown in Fig. 5. The experimental results suggest that cooling rate has a dominant effect on the precipitation behavior of TiN and TiN can precipitate from the melts at the initial stage of solidification if the cooling rate is sufficiently high. Therefore, it is not reasonable to predict the precipitation behavior of TiN only using equilibrium assumptions. Moreover, cooling rate affects the characteristics of TiN in the solidified microstructure greatly. There are many TiN precipitates in the water-cooled samples and the size of TiN is about 1 μm, as shown in Fig. 5(a). In the furnace-cooled samples, the size of TiN is about 10 μm, which is much coarser than that in the water-cooled samples, and the amount is decreased greatly, as shown in Fig. 5(c). The size of TiN for the air cooling samples is about 3 μm. High cooling rate can refine the solidified microstructure and make the microstructure more uniform in comparison with the common solidification techniques [29–31]. The surface scanning analyses of a precipitate indicate that the precipitate is mainly composed of Ti and N elements, as shown in Fig. 6(a) and (b). In the core of the precipitate, Ca and O elements are observed, as shown in Fig. 6(c) and (d), which means that CaO may act as the heterogeneous nucleation site of TiN. No Fe and Cr elements are found in the precipitate.

In the calculation of Figs. 2 and 3, interface composition is calculated based on phase diagram during solidification, which means that interface equilibrium is assumed. However, under rapid

Table 3
Solidification parameters used in this work [26–28].

Parameter	Ti	N	Reference
Equilibrium distribution coefficient, k_0	0.40	0.32	26
Liquidus slope, m_L (K/wt.%)	−20	−64.5	
Solute diffusion coefficient, D_L (cm^2/s)	7.3×10^{-5}	1.56×10^{-3}	27
Interatomic distance, α_0(cm)	2.0×10^{-7}		28
Velocity of sound for pure metals, V_0(cm^2/s)	4.0×10^{5}		28
Melting point of pure solvent, T_0 (K)	1789		
Liquidus, T_L (K)	1783		
Solidus, T_S (K)	1772		

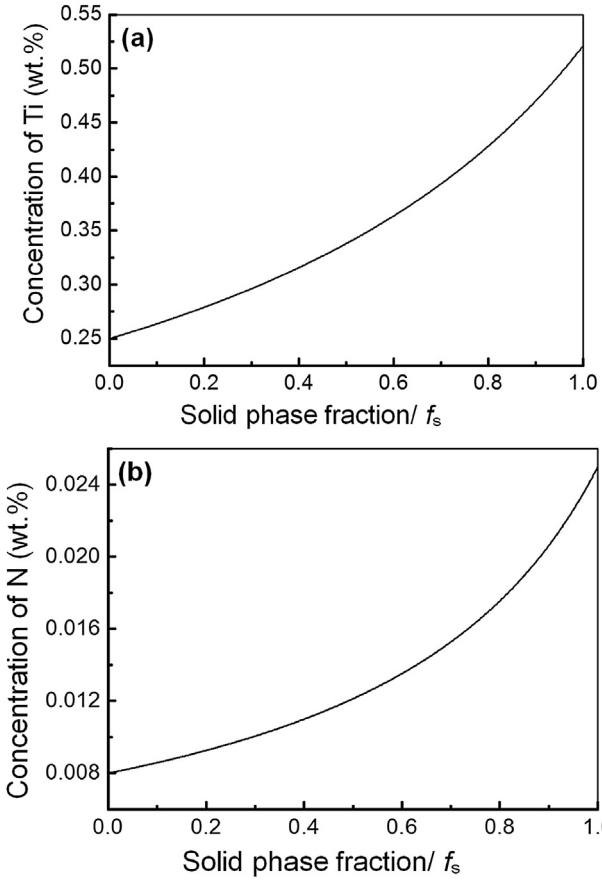

Fig. 2. The relationship between the solute concentration in the liquid at the solid/liquid interface and solid-phase fraction under equilibrium solidification for AISI 439 stainless steel. (a) for Ti solute; (b) for N solute.

solidification conditions, it is hard to achieve equilibrium, and interface composition and temperature cannot be determined by Equations (7) and (8). Therefore, non-equilibrium conditions should be taken into account because the solidification cannot operate under equilibrium in many casting conditions.

3.3. Precipitation of TiN during solidification under non-equilibrium conditions

It is known that solidification process of ferritic stainless steels is controlled by solute diffusion. Thus, cooling rate exhibits a dominant effect on the solidification behavior of ferritic stainless steels. When the cooling rate is much higher, there is no enough time for solute atoms to diffuse completely during solidification. Furthermore, the diffusibility in the solid is much lower than that in the

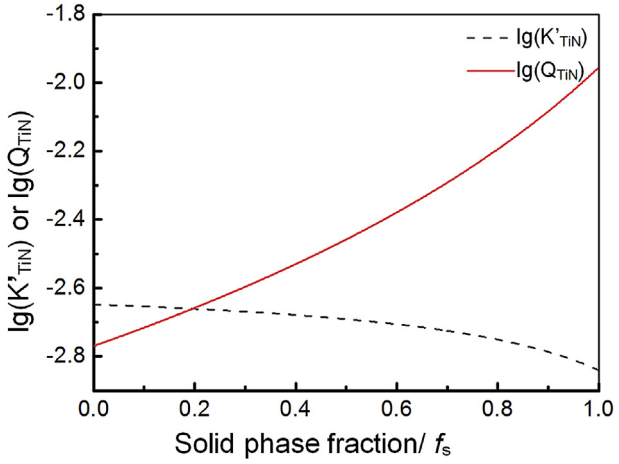

Fig. 3. The relationship between the concentration product of solutes Ti and N in the melts and the concentration product during equilibrium solidification.

liquid. Therefore, the composition in the solid cannot change following the solidus during solidification. A limiting case is that solute diffusion in the solid is negligible and the diffusion in the liquid remains complete. This non-equilibrium treatment method produces the following classical equation: [24]

$$C_S^* = k_0 C_0 (1 - f_S)^{(k_0 - 1)} \quad (9)$$

where C_S^* is the concentration in the solid at the solid/liquid interface. Equation (9) is often referred as the Scheil equation, which can be considered as a reasonable approximation when directional solidification and small volume element within the mushy zone dominate. In Equations (8) and (9), complete diffusion in the solid and no diffusion in the solid during solidification are assumed respectively. However, these assumptions are not in agreement with the real situation where solute diffusions appear but are not complete in the solid. So, the real solidification behavior should lie somewhere between the above two extremes.

The model by Brody and Flemings and Clyne and Kurz [22,23] is wildly used for the analyses of solute redistribution during alloy solidification. However, in Equations (8) and (9), equilibrium or local equilibrium solidification at the solid/liquid interface is assumed, where Gibbs free energy difference before and after solidification is equal to zero. When the cooling rate is high enough, non-equilibrium effect at the interface will dominate the solidification behavior, and deviation from local equilibrium occurs. The compositions in the solid and liquid at the interface are not unique and cannot be obtained by phase diagram directly. Here, the compositions in the solid and liquid at the interface can be analyzed by Gibbs free energy change during solidification. The relationship between Gibbs free energy and composition can be schematically

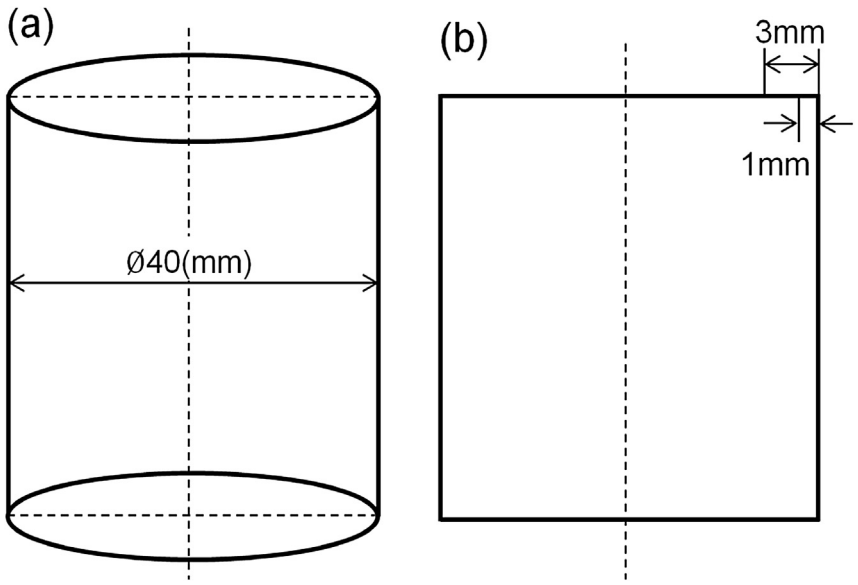

Fig. 4. Schematic of the cast samples showing the approximate site in samples corresponding to the images of Fig. 5.

shown in Fig. 7. At a given interface temperature T_i, the equilibrium compositions in the liquid C_{Le} and in the solid C_{Se} can be obtained by drawing a common tangent to the free energy curves for the liquid and solid. For a given liquid composition C_L, the free energy change can be determined by drawing a tangent at the composition C_L when 1 mol solid precipitates from an infinite amount of liquid with the composition C_L.

From Fig. 7, it is found that for the given liquid composition C_L, a range of the compositions of the formed solid are possible according to the decrease of Gibbs free energy. When the precipitated solid composition is assumed to be C_S, the free energy change for 1 mol solidified solid, ΔG_m, shown in Fig. 7, can be expressed as:

$$\Delta G_m = (1 - C_S)[\mu_{SA}(C_S) - \mu_{LA}(C_L)] + C_S[\mu_{SB}(C_S) - \mu_{LB}(C_L)] \tag{10}$$

where $\mu_{SA}(C_S)$, $\mu_{LA}(C_L)$, $\mu_{SB}(C_S)$, and $\mu_{LB}(C_L)$ are the chemical potentials of solvent and solute in the solid and liquid, respectively. For dilute solutions, the chemical potentials of solvent in the solid and liquid can be obtained according to Raoult law as:

$$\mu_{SA}(C_S) = \left[\mu_{SA}^{\Theta}(T) + RT\ln\left(P_A^*\right)\right] + RT\ln(1 - C_S) \tag{11}$$

$$\mu_{SA}^{0}(C_{Se}) = \left[\mu_{SA}^{\Theta}(T) + RT\ln\left(P_A^*\right)\right] + RT\ln(1 - C_{Se}) \tag{12}$$

$$\mu_{LA}(C_L) = \left[\mu_{LA}^{\Theta}(T) + RT\ln\left(P_A^*\right)\right] + RT\ln(1 - C_L) \tag{13}$$

$$\mu_{LA}^{0}(C_{Le}) = \left[\mu_{LA}^{\Theta}(T) + RT\ln\left(P_A^*\right)\right] + RT\ln(1 - C_{Le}) \tag{14}$$

where $\mu_{SA}^{0}(C_{Se})$ and $\mu_{LA}^{0}(C_{Le})$ are the chemical potentials of solvent in the solid and liquid under equilibrium conditions, respectively, $\mu_{SA}^{\Theta}(T)$ and $\mu_{LA}^{\Theta}(T)$ the standard chemical potentials at T temperature in the solid and liquid, respectively, and P_A^* the vapor pressure for pure solvent A at T temperature. Using $\mu_{SA}^{0}(C_{Se}) = \mu_{LA}^{0}(C_{Le})$ and Equations (11)–(14), (15) can be obtained as:

$$\mu_{SA}(C_S) - \mu_{LA}(C_L) = RT[\ln(1 - C_{Le}) - \ln(1 - C_{Se}) + \ln(1 - C_S) - \ln(1 - C_L)] \tag{15}$$

By using $\lim_{x\to 0}[\ln(1-x)] \approx -x$, Equation (15) can be simplified as:

$$\mu_{SA}(C_S) - \mu_{LA}(C_L) = RT[(C_L - C_{Le}) - (C_S - C_{Se})] \tag{16}$$

For solutes, using the similar method, Equation (17) can be obtained according to Henry law

$$\mu_{SB}(C_S) - \mu_{LB}(C_L) = RT\left[\ln\frac{C_{Le}C_S}{C_{Se}C_L}\right] \tag{17}$$

Substituting Equations (16) and (17) into (10), the Gibbs free energy change for forming 1 mol solid can be written as:

$$\frac{\Delta G_m}{RT} = (1 - C_S)[(C_L - C_{Le}) - (C_S - C_{Se})] + C_S\ln\frac{C_{Le}C_S}{C_{Se}C_L} \tag{18}$$

Using $k_0 = C_{Se}/C_{Le}$ and $k_v = C_S/C_L$, Equation (18) is changed as:

$$\frac{\Delta G_m}{RT} = (1 - k_V C_L)[(C_L - C_{Le}) - (k_V C_L - k_0 C_{Le})] + k_V C_L\ln\frac{k_V}{k_0} \tag{19}$$

For linear solidus and liquidus, the interface temperature can be expressed as:

$$T_i = T_0 + m_L C_{Le} \tag{20}$$

where m_L is the liquidus slope under equilibrium solidification conditions. Using Equations (19) and (20), the interface temperature can be expressed as:

$$T_i = T_0 + m_L\left[\frac{(1 - k_V)(1 - k_V C_L) + k_V\ln(k_V/k_0)}{(1 - k_0)(1 - k_V C_L)}\right]C_L - \frac{\Delta G_m m_L}{RT_i(1 - k_0)(1 - k_V C_L)} \tag{21}$$

According to [32], the mole free energy change can be expressed

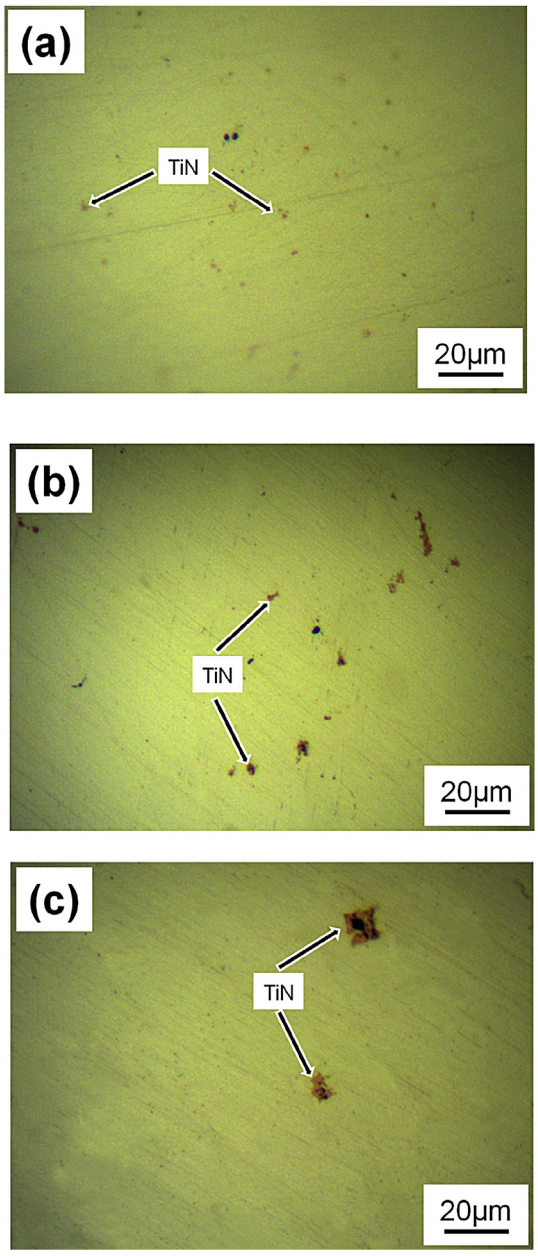

Fig. 5. TiN Morphology in the solidified microstructure under different cooling conditions. (a) at the surface of the sample cooled in water; (b) about 1 mm away from the surface of the sample cooled in air; (c) about 3 mm away from the surface of the sample cooled within the furnace.

as:

$$\Delta G_m = -RT_i \ln\left(1 - \frac{V}{V_0}\right) \tag{22}$$

where V is the growth rate of the interface and V_0 a constant which is of the order of the velocity of sound for pure metals. Using $\lim_{x\to 0}[\ln(1-x)] \approx -x$, Equation (22) can be written as:

$$\Delta G_m = RT_i V/V_0 \tag{23}$$

Substituting Equation (23) into (21), the interface temperature can be finally written as:

$$T_i = T_0 + m_L\left[\frac{(1-k_V)(1-k_V C_L) + k_V \ln(k_V/k_0)}{(1-k_0)(1-k_V C_L)}\right]C_L - \frac{Vm_L}{V_0(1-k_0)(1-k_V C_L)} \tag{24}$$

Now, the relationship between the temperature, composition at the solid/liquid interface and growth rate under non-equilibrium solidification conditions has been established. This equation can be extended into multicomponent alloys [33]. In order to calculate the interface temperature under non-equilibrium solidification, the parameter k_V should be known first. Using the reaction rate theory to correlate the atomic motions across the interface, Aziz [34] obtained the following equation:

$$k_V = \frac{k_0 + \alpha_0 V/D_L}{1 + \alpha_0 V/D_L} \tag{25}$$

where α_0 is of the order of interatomic distance and D_L the solute diffusion coefficient in the liquid.

From Equations (24) and (25), it is apparent that growth rate has an important effect on the interface temperature. The interface temperature is directly related with the undercooling which is the driving force for solidification. Thus, the change of interface temperature due to high growth rate during solidification is one of the main characteristics under non-equilibrium conditions. This can resultantly determine the precipitation behavior of TiN in ferritic stainless steels.

Another important characteristic of non-equilibrium solidification is the solute composition in the liquid at the solid/liquid interface, which cannot be determined by the phase diagram any more. In both Scheil and Brody-Flemings models, complete mixing in the liquid is assumed. However, under high cooling rate during solidification, it is impossible to achieve complete diffusion in the liquid without strong convection due to the time limit. In the model by Tiller et al. [35], no diffusion in the solid and only diffusion without convection in the liquid are assumed. For solute redistribution under rapid solidification, no diffusion in the solid can be assumed. It is reasonable under non-equilibrium solidification since the cooling rate is much higher and there is no enough time for solutes to diffuse in the solid. In the liquid, incomplete mixing during solidification should be assumed since residual convection by pouring and natural convection may exist. Similar with Brody-Flemings, the solute redistribution can be determined as Equation (26) by using solute conservation within the volume element, as shown in Fig. 8.

$$(C_L - C_S)Ldf_S = \frac{1}{2}\delta_L dC_L \tag{26}$$

where L is the length of the volume element and δ_L, solute boundary layer in the liquid, is given as:

$$\delta_L = \frac{2D_L}{V} \tag{27}$$

After calculating by integration, solute concentration in the liquid at the solid/liquid interface can be obtained as:

$$C_L = C_0.\exp\left[\frac{VL}{D_L}(1-k_V)f_S\right] \tag{28}$$

Equation (28) relates the solute composition in the liquid at the solid/liquid interface with the solid-phase fraction and growth rate.

Now, the influence of non-equilibrium effect on the composition and temperature at the solid/liquid interface can be discussed. Using Equation (25), (28) and the parameters listed in Table 3

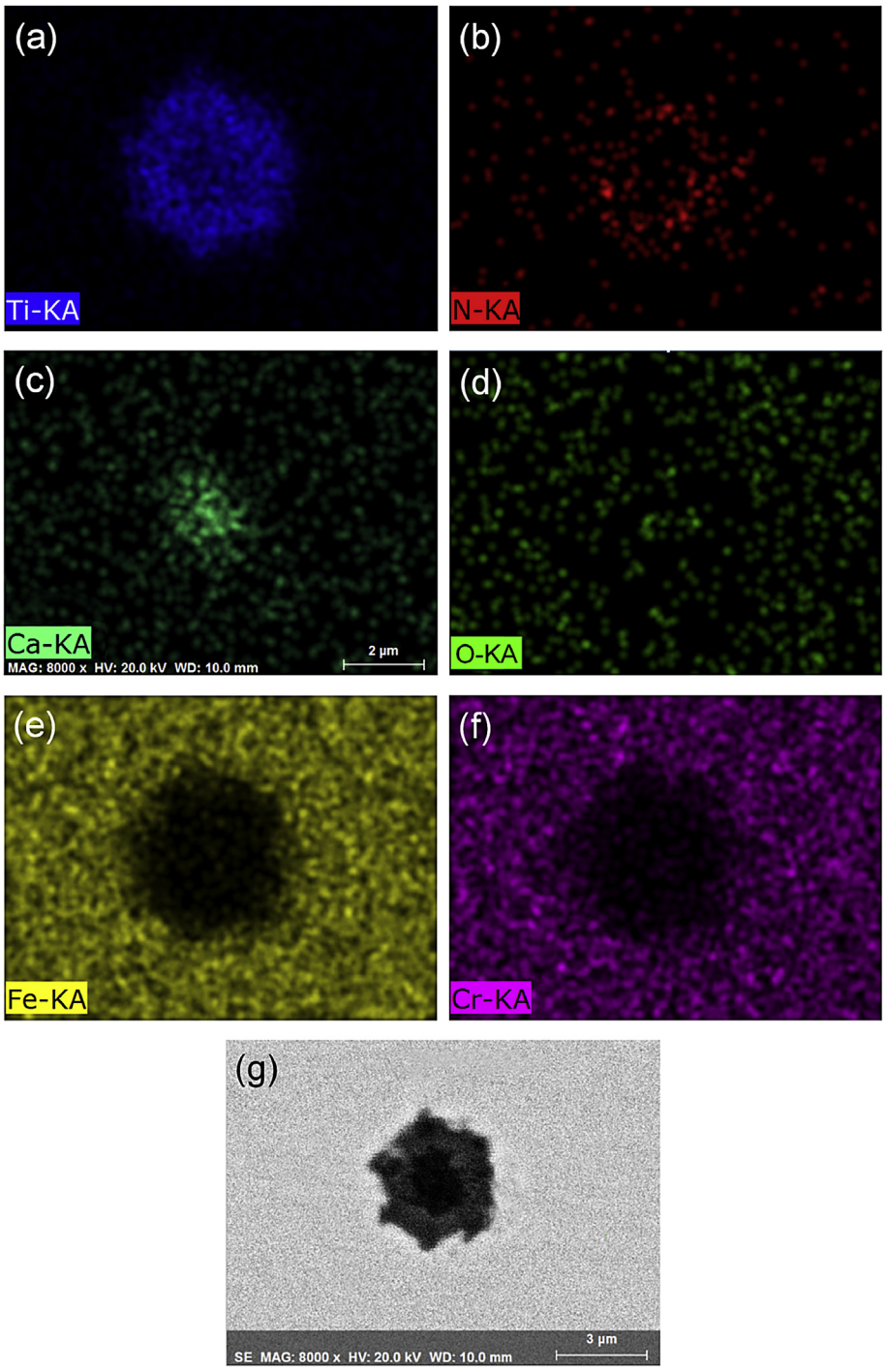

Fig. 6. Surface scanning analysis of TiN precipitate in the steel. (a) Ti; (b) N; (c) Ca; (d) O; (e) Fe; (f) Cr; (g) SEM image.

[26–28], the relationship between the solute concentration in the liquid at the solid/liquid interface and the solidification length under various growth rates can be obtained, as shown in Fig. 9. It can be found that the concentrations of Ti and N solutes in the liquid at the solid/liquid interface increase significantly at the initial stage. Subsequently, a steady value will be reached at a certain solidification length. With the further increase of the solidification length, solute concentrations in the liquid at the solid/liquid interface almost remain unchanged. Furthermore, the solidification length before steady solute concentration is shortened markedly with increasing the growth rate. This indicates that solute concentrations of Ti and N can reach a steady value immediately at a very short solidification length when a high growth rate is imposed. For the present stainless steel, at the growth rate of 10 cm/s, the solute concentration of Ti and N can rise up to a steady value immediately at the initial stage of solidification, as shown in Fig. 9. Meantime, the solute concentration (C_L) required to form TiN under non-equilibrium solidification is lower than the concentration under equilibrium solidification (C_{Le}), as shown in Fig. 7. Therefore, TiN can form at a very short solidification length if the growth rate

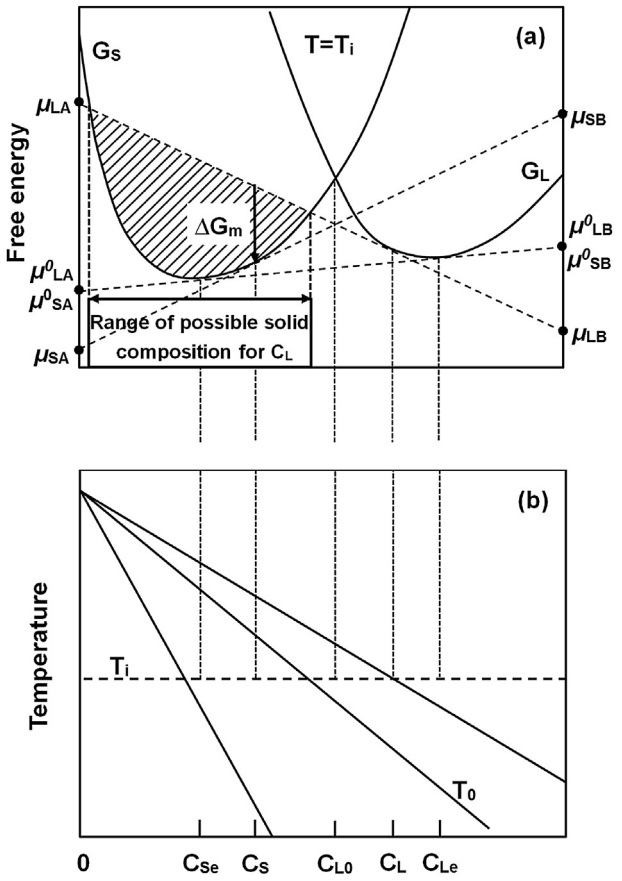

Fig. 7. Schematic diagram for establishing the relationship between the interface temperature, interface composition and the growth rate considering non-equilibrium effect (possible range to form solid C_S from C_L liquid composition is denoted).

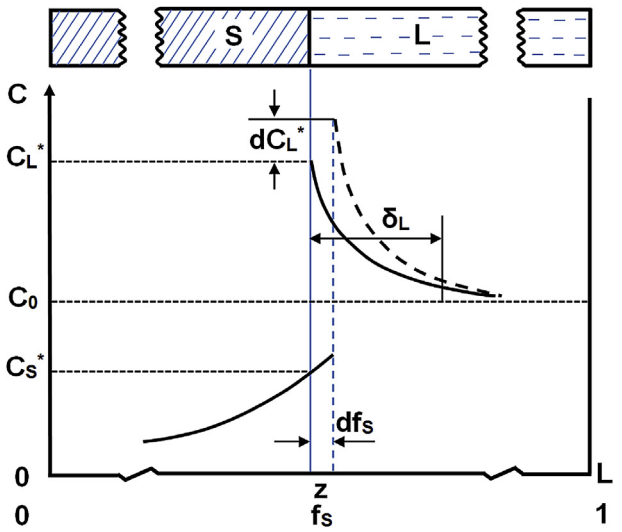

Fig. 8. Schematic illustration of the solute redistribution during directional solidification.

is sufficiently high. This can account for the observed TiN at the surface of the water-cooled samples, as shown in Fig. 5(c).

Based on Equations (24), (28) and the parameters listed in Table 3, the effect of growth rate on the temperature at the solid/liquid interface during solidification can be discussed as well. Fig. 10

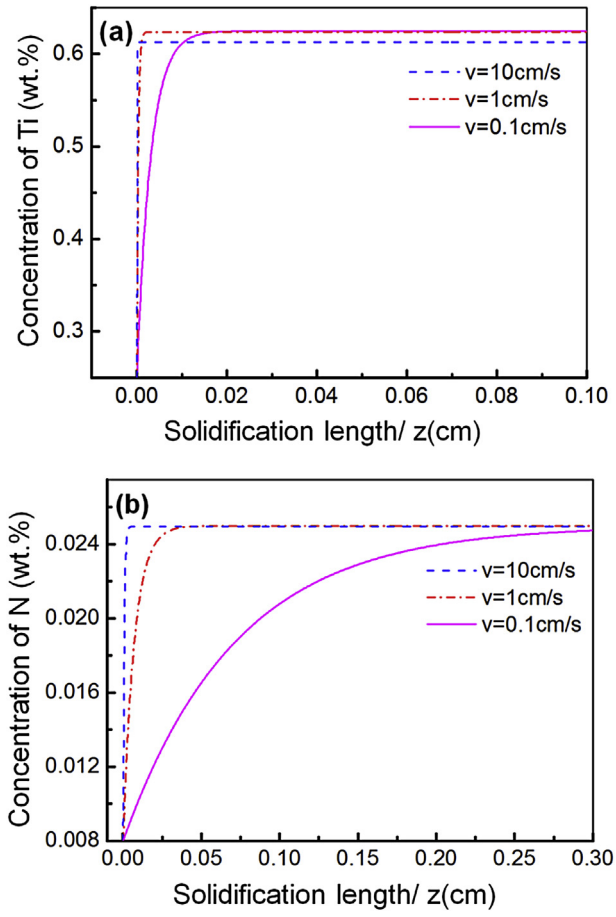

Fig. 9. The relationship between the solute concentration in the liquid at the solid/liquid interface and the solidification length under various growth rates. (a) for Ti solute; (b) for N solute.

shows the relationship between the interface temperature and solidification length at various growth rates. It is apparent that the temperature at the solid/liquid interface decreases gradually with the increase of the solidification length and then reaches a plateau at a certain solidification length. Furthermore, growth rate has a significant effect on the temperature at the solid/liquid interface during solidification. With the increase of the growth rate, the temperature at the solid/liquid interface is decreased more rapidly. Meanwhile, the corresponding solidification length becomes shorter when the temperature at the solid/liquid interface approaches the plateau. It is known that the concentration of Ti and N in the melts is lowered when the interface temperature is decreased. It is more favorable for TiN to precipitate from the melts at higher growth rate during solidification due to lower interface temperature and shorter solidification length. The interface temperature is decreased to the plateau when the solidification length is almost zero at the growth rate of 10 cm/s for the present stainless steel. This suggests that TiN can precipitate from the melts in the initial stage of solidification at the growth rate of 10 cm/s, which is in agreement with the observed TiN in the water-cooled samples, as shown in Fig. 5(c). Compared with the prediction using equilibrium approach, as shown in Fig. 3, this model is more precise in the prediction of TiN precipitation in ferritic stainless steel since non-equilibrium solidification has been considered. It should be noted that though the calculated results in Figs. 9 and 10 show that TiN can form at the initial stage of solidification at the growth rate of 10 cm/s and TiN can be observed at the surface of the water-

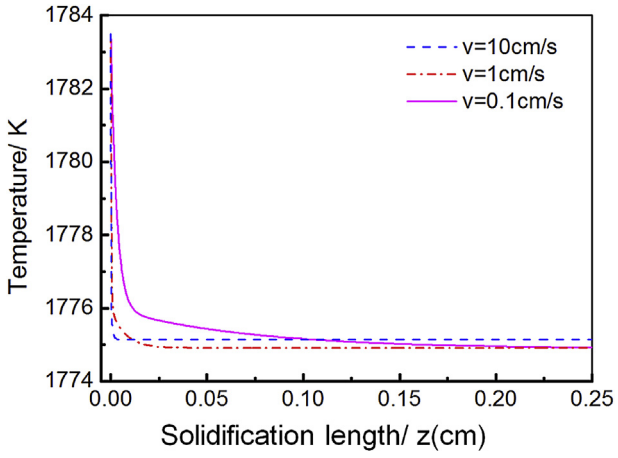

Fig. 10. The change of the temperature at the solid/liquid interface with the solidification length under various growth rates.

cooled samples, actual growth rate cannot be measured directly. Therefore, the calculated results in Figs. 9 and 10 cannot be linked directly to the experimental observations of the water-cooled samples at present.

4. Conclusions

In summary, the main conclusions drawn from this work can be shown as follows:

(1) According to the calculations using equilibrium approaches, TiN cannot precipitate directly in the melts and can form when the solid-phase fraction reaches 0.2 during solidification.

(2) Taking into account the non-equilibrium conditions, a model, relating the interface temperature with the interface composition and growth rate, was developed as $T_i = T_0 + m_L\left[\frac{(1-k_V)(1-k_V C_L)+k_V \ln(k_V/k_0)}{(1-k_0)(1-k_V C_L)}\right]C_L - \frac{Vm_L}{V_0(1-k_0)(1-k_V C_L)}$.

(3) The calculations using this model show that TiN can precipitate when the solidification length is very low at the growth rate of 10 cm/s for the present AISI 439 ferritic stainless steel. This result is in agreement with the experimental work where TiN was observed at the surface of the water-cooled samples.

Acknowledgements

This work was financially supported by the National Natural Science Foundation of China (No. 51571081).

References

[1] K.H. Lo, C.H. Shek, J.K.L. Lai, Recent developments in stainless steels, Mater. Sci. Eng. R. 65 (2009) 39–104.
[2] H. Yan, H. Bi, X. Li, Z. Xu, Microstructure and texture of Nb+Ti stabilized ferritic stainless steel, Mater. Character 59 (2008) 1741–1746.
[3] J. Han, H. Li, Z. Zhu, L. Jiang, H. Xu, L. Ma, Effects of processing optimization on microstructure, texture, grain boundary and mechanical properties of Fe-17Cr ferritic stainless steel thick plate, Mater. Sci. Eng. A 616 (2014) 20–28.
[4] J. Han, H. Li, F. Barbaro, L. Jiang, Z. Zhu, H. Xu, L. Ma, Precipitation and impact toughness of Nb-V stabilized 18Cr-2Mo ferritic stainless steel during isothermal aging, Mater. Sci. Eng. A 612 (2014) 63–70.
[5] M.S. Khorrami, M.A. Mostafaei, H. Pouraliakbar, A.H. Kokabi, Study on microstructure and mechanical characteristics of low-carbon steel and ferritic stainless steel joints, Mater. Sci. Eng. A 608 (2014) 35–45.
[6] Hoon-Hwe Cho, H.N. Han, Sung-Tae Hong, Jong-Hwan Park, Yong-Jai Kwon, Seok-Hyun Kim, Russell J. Steele, Microstructural analysis of friction stir welded ferritic stainless steel, Mater. Sci. Eng. A 528 (2011) 2889–2894.
[7] Hyung-Joon Shin, Joong-Kyu An, S.H. Park, D.N. Lee, The effect of texture on ridging of ferritic stainless steel, Acta Mater 51 (2003) 4693–4706.
[8] J.H. Park, J.K. Kim, B.H. Lee, S.S. Kim, K.Y. Kim, Three-dimensional atom probe analysis of intergranular segregation and precipitation behavior in Ti-Nb-stabilized low-Cr ferritic stainless steel, Scr. Mater 68 (2013) 237–240.
[9] A. Malfliet, F. Verhaeghe, F. Chassagne, J.D. Mithieux, B. Blanpain, P. Wollants, Precipitation in Fe-15Cr-1Nb alloys after oxygenation, Acta Mater 58 (2010) 3832–3841.
[10] J. Han, H.J. Li, Z.X. Zhu, F. Barbaro, L.Z. Jiang, H.G. Xu, L. Ma, Microstructure and mechanical properties of friction stir welded 18Cr-2Mo ferritic stainless steel thick plate, Mater. Des. 63 (2014) 238–246.
[11] G.K. Tirumalasetty, M.A. van Huis, C.M. Fang, Q. Xu, F.D. Tichelaar, D.N. Hanlon, J. Sietsma, H.W. Zandbergen, Characterization of NbC and (Nb, Ti)N nano-precipitates in TRIP assisted multiphase steels, Acta Mater 59 (2011) 7406–7415.
[12] K. Nakajima, H. Hasegawa, S. Khumkoa, M. Hayashi, Effect of catalyst on heterogeneous nucleation in Fe-Ni-Cr alloys, ISIJ. Int. 46 (2006) 801–806.
[13] C. Shi, G. Cheng, Z. Li, P. Zhao, Solidification structure refining of 430 ferrite stainless steel with TiN nucleation, J. Iron Steel Res. Int. 15 (2008) 57–60.
[14] X. Li, Q. Cai, B. Zhao, Y. Xiao, Bing Li, Effect of nano TiN/Ti refiner addition content on the microstructure, and properties of as-cast Al-Zn-Mg-Cu alloy, J. Alloy. Compd. 675 (2016) 201–210.
[15] F. Weng, H. Yu, C. Chen, J. Liu, L. Zhao, Microstructures and properties of TiN reinforced Co-based composite coatings modified with Y_2O_3 by laser cladding on Ti-6Al-4V alloy, J. Alloy. Compd. 650 (2015) 178–184.
[16] S. Jonsson, Assessment of the Fe-Ti-C system, calculation of the Fe-Ti-N system, and prediction of the solubility limit of Ti(C, N) in liquid Fe, Metall. Mater. Trans. B 29 (1998) 371–384.
[17] Bahri Ozturk, R. Matway, R.J. Fruehan, Thermodynamics of inclusion foumation in Fe-Cr-Ti-N alloy, Metall. Mater. Trans. B 26 (1995) 563–567.
[18] W.Y. Kim, J.O. Jo, T.I. Chung, D.S. Kim, J.J. Pak, Thermodynamics of titanium, nitrogen and TiN formation in liquid iron, ISIJ. Int. 47 (2007) 1082–1089.
[19] J.J. Pak, Y.S. Jeong, I.K. Hong, W.Y. Cha, D.S. Kim, Y.Y. Lee, Thermodynamics of TiN formation in Fe-Cr melts, ISIJ. Int. 45 (2005) 1106–1111.
[20] J. Fu, J. Zhu, L. Di, F. Tong, Study on the precipitation behavior of TiN in the microalloyed steels, Acta Metall. Sin. 36 (2000) 801–804.
[21] D. Zhou, J. Fu, X. Chen, J. Li, Precipitation behavior of TiN in bearing steel, J. Mater. Sci. Technol. 19 (2003) 184–186.
[22] H.D. Brody, M.C. Flemings, Solute distribution during dendritic solidifiction, Trans. Metall. Soc. AIME 236 (1966) 615–624.
[23] C. Wagner, Thermodynamics of Alloys, Addison-Wesly Press, Cambridge, Mass, 1952, pp. 47–51.
[24] T.W. Clyne, W. Kurz, Solute redistribution during solidification with rapid solid state diffusion, Metall. Trans. A 12 (1981) 965–971.
[25] Z.T. Ma, D. Janke, Characteristics of oxide precipitation and growth during solidification of deoxidized steel, ISIJ. Int. 38 (1998) 46–52.
[26] Joint Society on Iron and Steel Basic Research, Solidification of Iron and Steel, Tokyo, 1977.
[27] Е. Фромм, Е. Гебхардт, Газы И Углерод В Металлах, Металлургия, Москва, 1980.
[28] T. Umeda, T. Okane, W. Kurz, Phase selection during solidification of peritectic alloys, Acta Mater 44 (1996) 4209–4216.
[29] X. Huang, N.H. Pryds, Crystallography and morphology of cementite precipitates formed during rapid solidification of a ferritic stainless steel, Acta Mater 48 (2000) 4073–4082.
[30] R. Trivedi, W. Kurz, Morphological stability of a planer interface under rapid solidification conditions, Acta Mater 34 (1986) 1663–1670.
[31] D.M. Herlach, Non-equilibrium solidification of undercooled metallic melts, Mater. Sci. Eng. R12 (1994) 177–272.
[32] R. Trivedi, W. Kurz, Dendritic growth, Inter. Mater. Rev. 39 (1994) 49–74.
[33] U. Hecht, L. Gránásy, T. Pusztai, B. Böttger, M. Apel, V. Witusiewicz, L. Ratke, J. De Wilde, L. Froyen, D. Camel, B. Drevet, G. Faivre, S.G. Fries, B. Legendre, S. Rex, Multiphase solidification in multicomponent alloys, Mater. Sci. Eng. R. 46 (2004) 1–49.
[34] M.J. Aziz, Model for solute redistribution during rapid solidification, J. Appl. Phys. 53 (1982) 1158–1168.
[35] W.A. Tiller, K.A. Jackson, J.W. Rutter, B. Chalmers, The redistribution of solute atoms during the solidification of metals, Acta. Metall. 1 (1953) 428–437.